Ab initio calculations of the mechanical and electronic properties of strained Si nanowires

Paul W. Leu,* Alexei Svizhenko,† and Kyeongjae Cho‡
Stanford University, Stanford, California 94305, USA

(Received 5 September 2007; revised manuscript received 14 March 2008; published 9 June 2008)

This paper reports a systematic study of the mechanical and electronic properties of strained small diameter (0.7–2.6 nm) silicon nanowires (Si NWs) using *ab initio* density functional theory calculations. The values of Young's modulus, Poisson ratio, band gap, effective mass, work function, and deformation potentials are calculated for ⟨110⟩ and ⟨111⟩ Si NWs. We find that quantum confinement in ⟨110⟩ Si NWs splits conduction band valleys and decreases transport effective mass compared to the bulk case. Consequently, additional tensile strain should not lead to further significant electron mobility improvement. An interesting finding we report in this paper is that under compressive strain, there is a dramatic decrease in deformation potentials of ⟨110⟩ Si NWs, which may result in a strong increase in electron mobilities, despite a concurrent increase in effective mass. We also observe a similar strain-induced counterplay of hole deformation potentials and effective masses for both ⟨110⟩ and ⟨111⟩ Si NWs. Finally, we do not see any significant effect of tensile or compressive strain on electron effective masses and deformation potentials in ⟨111⟩ Si NWs. The sudden changes in effective mass and deformation potentials are concurrent with a change in the conduction and valence band edge states. In ⟨110⟩ NWs, this change corresponds to a transition from direct-to-indirect band gap under strain.

DOI: 10.1103/PhysRevB.77.235305 PACS number(s): 78.67.Lt, 73.21.Hb, 73.22.−f, 31.15.A−

I. INTRODUCTION

Semiconductor nanowires (NWs) have the potential for a variety of nanoelectromechanical system and nanodevice applications. Many NW electronic devices have been experimentally demonstrated. A number of theoretical studies have been performed on Si NWs, such as the effect of structure,[1–3] surface passivation,[4] orientation and surface roughness,[5] defects,[6] morphology and doping.[7] The theoretical study of the effects of strain on bulk Si has been reported.[8] Some tight binding calculations have been performed on the effects of strain in GaAs NWs,[9] and numerous theoretical studies have been done on strained carbon nanotubes.[10–14] However, the effects of strain on Si NW electronic structure has not been systematically investigated.[15]

Strain plays an important role in the electronic and optical properties of Si NWs. Si NWs grown within mesoporous silica pores have exhibited up to 2% strain and shown a shift in photoluminescence suggestive of strain-induced band structure changes.[16,17] The effect of strain on optical band gap in GaN NWs has also been observed.[18] In a recent paper it was demonstrated that Si NWs have a piezoresistance a few orders of magnitude greater than that of bulk Si.[19] Strain has been used within planar Si metal-oxide-semiconductor field-effect transistors to enhance mobility by reducing electron intervalley scattering and redistributing carriers within conduction valleys to lower effective mass.[20] Strain strongly affects the resistivity of bulk Si and its piezoresistance has been used for a variety of strain, pressure, and acceleration sensor applications.

A variety of experimental techniques, such as x-ray diffraction,[21] high resolution transmission electron microscopy,[22,23] and cantilever deflection,[24] have been used for characterizing strain within NWs. NWs can accommodate large amounts of strain due to the high energy cost of forming defects in such small structures. Recent experiments have measured a maximum yield strength corresponding to about 13% strain in Ge NWs, where the NWs fail without plastic deformation.[25] Experiments over many Si NWs between 100 and 200 nm in diameter resulted in an average yield strength of 6.3% strain, with some fracturing at 10% strain.[26] A Si NW less than 10 nm in diameter was shown to have an elastic limit of $10 \pm 2\%$ strain and a fracture strain of $30 \pm 1\%$.[27] Molecular dynamics simulations on Si NWs have also suggested very high yield strengths above 10%.[28]

Strain is present or can be applied to Si NWs in a variety of ways. Si NWs tend to form an amorphous SiO_2 layer of 1–2 nm thickness upon exposure to air,[29] and this oxide layer should induce compressive radial strain and tensile axial strain within the NW.[30] Molecular dynamics simulations[31] and continuum analysis[32] have suggested the values of strain on the order of a few percent in Si NWs due to Si oxide. Surround gate Si NW field-effect transistors should be affected by strain due to the gate oxide.[33,34] NWs can also experience strain through surface stresses or lattice mismatch with the catalyst or substrate, or from its surrounding medium. Coaxial NWs[35] or striped NWs[36–38] should experience strain due to lattice mismatch between the different materials used. Epitaxial coaxial Si Ge NWs should have up to a few percent strain due to the lattice mismatch between Si and Ge. NWs may also be deformed externally from an atomic force microscope or scanning tunneling microscope, or applied on bridged NWs.[39] Some theoretical studies have been performed on the electronic structure of oxidized Si nanoparticles[40,41] and epitaxial core-shell NWs.[42]

Strain is important in Si technology and applications as a means to enhance electron or hole mobility. In the relaxation time approximation, the mobility is affected by the effective mass $m_{e,h}$ and the deformation potential E_a,

$$\mu_{e,h} = \frac{e\langle \tau \rangle}{m_{e,h}} \propto \frac{1}{E_a^2 m_{e,h}}. \quad (1)$$

Therefore, a smaller effective mass or deformation potential would immediately mean higher currents and better device

 ©2008 The American Physical Society

performance. Moreover, lower effective masses and higher velocities would mean a weaker sensitivity of carriers to surface roughness scattering,[5] which is an important factor in NWs and other one-dimensional structures. In bulk Si under biaxial tensile strain in ⟨100⟩ or uniaxial tensile strain in ⟨110⟩ directions, an increase in electron mobility is achieved by strain-induced splitting of conduction band valleys, which leads to the redistribution of electrons to the Δ_2 valleys with a lower effective mass in the transport direction. A compressive strain in the same direction leads to an opposite effect. According to this picture, strain in the ⟨111⟩ direction does not affect electron mobilities, as all the six valleys of Si are equally affected and no electron redistribution occurs. The analysis is more complicated for the valence bands, where an interplay between the change in the effective mass, deformation potential, and matrix elements for inter-sub-band scattering result in changes of mobility. In this paper, we limit the discussion of mobility to the behavior of the effective mass and deformation potentials.

This paper is organized as follows: In Sec. II we discuss methods used which is followed by a discussion of mechanical and electronic properties of Si NWs under zero strain. In Sec. IV we report the effects of strain on band structure, band gap, effective mass, deformation potential, and work function of Si NWs. The implications of the combined behavior of these quantities under strain on electron and hole mobilities are discussed.

II. ATOMIC MODEL OF Si NANOWIRES AND CALCULATION METHODS

We employed *ab initio* density functional theory (DFT) calculations in order to study the effect of uniaxial tensile and compressive stress on the mechanical and electronic properties of Si NWs. We studied ⟨110⟩ and ⟨111⟩ Si NWs from 0.7 to 2.6 nm in diameter. We found that Young's modulus decreases and equilibrium axial lattice constant increases with decreasing size due to the contribution of surface effects. The increase in equilibrium axial lattice constant is more significant for ⟨110⟩ NWs, and the softening of Young's modulus is more significant in ⟨111⟩ NWs. Strain can be used to modify the band gap and work functions of Si NWs. Strain can cause a change in valence and conduction band edge states, leading to a direct-to-indirect band gap transitions, along with associated jumps in effective mass and deformation potentials. This implies the possibility of achieving a manyfold increase in electron and hole mobilities of Si NWs under strain due to a dramatic decrease in deformation potential.

In accordance with experimental observations[43] and Wulff construction,[44] the NWs were cut out of bulk Si using the low free-energy {111}, {100}, and {110} facets. The cross sections of NWs are illustrated in Fig. 1. The ⟨110⟩ NWs consist of two atomic planes per unit cell. The four ⟨110⟩ NWs under consideration, labeled 1–4 in Fig. 1, have, respectively, 2 Si and 4 H, 12 Si and 8 H, 27 Si and 12 H, and 48 Si and 16 H in each layer. The ⟨111⟩ NWs consist of six atomic planes per unit cell. Table I displays the number of Si and H atoms in each plane within a unit cell for the four ⟨111⟩ NWs under

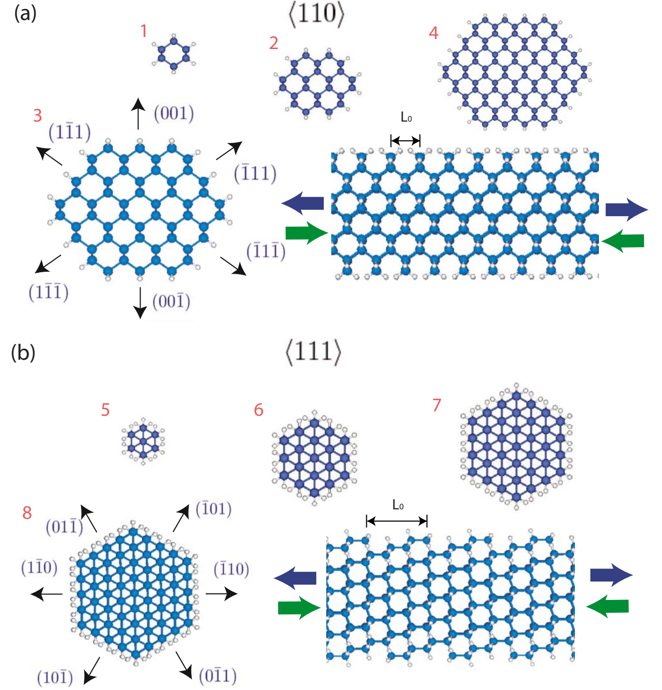

FIG. 1. (Color online) Cross section for (a) ⟨110⟩ and (b) ⟨111⟩ NWs. The labels of the NWs correspond to those in Table II. The side view of the NWs about 2 nm in diameter are shown.

consideration, labeled 5–8 in Fig. 1. All {111} and {110} facets were passivated by a single H atom for each Si atom, while the {100} facets were passivated with two H bonds for each Si atom to form a dihydride. The enumeration of NWs in Fig. 1 corresponds to that in Table II, which shows the number of atoms per unit cell and the diameter and equilibrium unit cell length of relaxed structures.

The calculations were done using DFT within the generalized gradient approximation (GGA)[45] with projector augmented wave pseudopotentials[46] using the Vienna *Ab Initio* Simulation Package (VASP). The simulation parameters were tested for convergence and similar to values used previously.[4,47] The NWs were placed in unit cells such that the interwire distance is greater than 10 Å, which effectively prevents the overlapping of wave functions from neighboring cells. The Kohn–Sham single-electron wave functions were expanded by plane waves with a cut-off energy of 400 eV. We used four Monkhorst–Pack k points along the axis of the NW. Strain was applied by increasing or decreasing the supercell size along the NW axis and then relaxing the geometry until the forces on each atom are less than 0.01 eV/Å.

III. EQUILIBRIUM PROPERTIES OF ⟨110⟩ AND ⟨111⟩ NWS

Table II shows some of the main results for the eight Si NWs that we have simulated. Y is Young's modulus, ν is the Poisson ratio, E_g is the band gap, WF is the work function, m_e and m_h are the electron and hole effective masses, respectively, and $\frac{\partial E_c}{\partial \varepsilon}$ and $\frac{\partial E_v}{\partial \varepsilon}$ are the deformation potentials of the conduction and valence band, respectively. NWs 1–4 are ⟨110⟩ oriented and 5–8 are ⟨111⟩ oriented.

TABLE I. Number of Si and H atoms in each layer of the ⟨111⟩ NWs.

	No. of atoms (Si; H)					
Wire no.	Layer 1	Layer 2	Layer 3	Layer 4	Layer 5	Layer 6
5	1; 0	1; 0	3; 6	3; 3	3; 3	3; 6
6	7; 6	7; 6	6; 3	6; 6	6; 6	6; 3
7	13; 9	13; 9	12; 6	12; 6	12; 6	12; 6
8	19; 6	19; 6	21; 12	21; 9	21; 9	21; 12

A. Mechanical properties

In Table II, the wire diameter was calculated from the wire area, where we defined the wire area by using the edges defined by the H atoms on each facet. The unit cell equilibrium lengths L_0 were determined from finding the minimum L by using a second order polynomial fit of total energy versus cell length.

The Young's modulus Y, the ratio between stress and strain ϵ, was calculated from $Y=\frac{1}{V_0}\frac{\partial^2 E}{\partial\epsilon^2}$, where $\frac{\partial^2 E}{\partial\epsilon^2}$ is the second derivative of the total energy with respect to the strain of the NW and V_0 is the minimum total energy volume. The Young's modulus Y of Si NWs has been measured in several experiments. $Y=18\pm 2$ GPa has been reported for a <10 nm diameter ⟨100⟩ Si NW.[27] Young's modulus for 60–200 nm diameter ⟨111⟩ Si NWs has been reported to be about the value for bulk Si.[48] In addition, the Young's modulus of ⟨001⟩ Si NWs has been calculated and it has been determined that Young's modulus decreases as the surface area with volume ratio increases.[47] The Poisson ratio ν is defined as $\nu=\frac{1}{\epsilon}\frac{R-R_0}{R_0}$, where R_0 is the minimum free-energy radius of the NW and R is the radius at strain ϵ. Table III displays the Poisson ratios $\nu_{[110],[1\bar{1}1]}$ and $\nu_{[110],[001]}$ for the various ⟨110⟩ NWs.

Young's modulus and the Poisson ratio are defined within a continuum mechanics framework. We looked at the sensitivity of Young's modulus and the Poisson ratio to our definition of wire radius. We consider how these mechanical properties change given some new definition of radius $r_0+\delta r_0$ instead of r_0. For Young's modulus, $Y'\approx Y(1-\frac{2\delta r_0}{r_0})$, where the prime indicates the value associated with radius $r_0+\delta r_0$.[47] Young's modulus is modified by an additional term $\frac{2\delta r_0}{r_0}$ that goes to 0 for larger wires (as $r_0\to\infty$). However, the Poisson ratio is more sensitive to the definition of radius: $\nu'\approx\nu(1-\frac{\delta r_0}{r_0}+\frac{\delta r-\delta r_0}{r-r_0})$. For the Poisson ratio, there is also a term $\frac{\delta r_0}{r_0}$ that goes to 0 as $r_0\to\infty$. However, there is an additional term $\frac{\delta r-\delta r_0}{r-r_0}$ that is present regardless of the size of the NW and can be significant as $r-r_0$ is typically small.

For reference, we calculated the bulk Si elasticity constants by DFT using projector augmented wave pseudopotentials[46] within the GGA by Perdew *et al.*[49] for comparison. We used a Monkhorst–Pack k-point mesh of $16\times 16\times 16$ with an energy cutoff of 400 eV. The free energy of the crystal was converged to within 0.01 eV with this k-point mesh. The equilibrium lattice constant of the bulk Si was 5.46 Å. We apply small strains to the equilibrium Si lattice and calculate the elastic constants from the resulting change in energy. Using Einstein summation notation, the energy of a crystal under strain $\boldsymbol{\epsilon}$ is

$$E(V,\boldsymbol{\epsilon})=E(V_0)+V_0\sigma_i\epsilon_i+V_0C_{ij}\epsilon_i\epsilon_j/2+\cdots, \quad (2)$$

where σ_i is the stress vector, ϵ_i is the strain vector, V_0 is the equilibrium volume, and C_{ij} is the elasticity matrix term. Voigt notation has been used where the symmetry properties of the stress, strain, and elasticity tensors have been used to collapse the indices using $xx\equiv 1$, $yy\equiv 2$, $zz\equiv 3$, $yz\equiv 4$, $zx\equiv 5$, and $yx\equiv 6$ and form the corresponding stress and vectors and elasticity matrix.

TABLE II. Various properties of the eight NWs simulated. Y is Young's modulus, ν is the Poisson ratio, E_g is the band gap, WF is the work function, m_e and m_h are the electron and hole effective masses, respectively, and $\frac{\partial E_c}{\partial\varepsilon}$ and $\frac{\partial E_v}{\partial\varepsilon}$ are the deformation potentials of the conduction and valence bands, respectively.

Wire no.	Growth direction	No. of atoms (Si; H)	Diameter (Å)	L_0 (Å)	Y (GPa)	ν	E_g (eV)	WF (eV)	$\frac{\partial(\mathrm{WF})}{\partial\varepsilon}$ (eV)	m_e (m_0)	m_h (m_0)	$\frac{\partial E_c}{\partial\varepsilon}$ (eV)	$\frac{\partial E_v}{\partial\varepsilon}$ (eV)
1	⟨110⟩	6; 8	6.6	4.04	139	0.13	2.63	4.65	9.0	0.14	0.19	−10.4	−7.6
2	⟨110⟩	24; 16	13.0	3.96	145	0.15	1.46	4.50	8.5	0.14	0.16	−10.1	−7.9
3	⟨110⟩	54; 24	19.4	3.92	150	0.16	1.11	4.42	9.2	0.08	0.09	−10.3	−8.1
4	⟨110⟩	96; 32	25.8	3.90	153	0.16	0.96	4.41	8.2	0.08	0.10	−9.6	−8.5
5	⟨111⟩	14; 18	6.5	9.52	43	0.05	3.43	4.14	1.95	2.6	0.58	−3.1	−3.9
6	⟨111⟩	38; 30	10.6	9.49	100	0.09	2.26	4.14	1.68	4.9	0.28	−4.4	−4.4
7	⟨111⟩	74; 42	14.7	9.48	118	0.11	1.68	4.18	2.25	4.9	0.64	−5.1	−5.8
8	⟨111⟩	122; 54	18.7	9.47	131	0.12	1.36	4.20	2.18	5.3	0.53	−5.1	−6.6

TABLE III. Poisson ratio of the ⟨110⟩ NWs along specific crystal directions.

Wire no.	$\nu_{[110],[001]'}$	$\nu_{[110],[1\bar{1}1]'}$
1	0.23	0.14
2	0.28	0.14
3	0.25	0.14
4	0.20	0.10

For Si, there are three independent elastic constants, C_{11}, C_{12}, and C_{44}, so we perform three different strains to obtain these elastic constants. We strain an eight atom unit cell bulk Si lattice with independent deformations (a) $\epsilon_1=\delta$, (b) $\epsilon_6=2\delta$, and (c) $\epsilon_1=\delta$, $\epsilon_2=-\delta$ using $\delta=\pm.005, \pm.01$. In each of the three cases, all other strain components are equal to 0. The atoms are relaxed within the unit cell until all forces are <0.01 eV/Å. The expressions for crystal free energy in Eq. (2) due to these strains are then fit with a second order polynomial to extract the elastic constants. Table IV displays the results of these calculations and compares them with experimental results from the literature. The results we have obtained are in good agreement with experimental results.[50]

Figure 2 displays the equilibrium axial lattice constant L_0 and Young's modulus of the NWs as a function of size. The equilibrium axial lattice constant was fit by the curve $C_1/d+C_2/d^2$ and Young's modulus was fit by $1-D_1/d-D_2/d^2$, where C_1 and D_1 are in Å and C_2 and D_2 are in Å^2. $C_1=22.0$ and $C_2=73.0$ for ⟨110⟩ NWs and $C_1=2.0$ and $C_2=4.7$ for ⟨111⟩ NWs. We obtained $D_1=0.9$ and $D_2=0.0$ for ⟨110⟩ NWs and $D_1=4.5$ and $D_2=2.4$ for ⟨111⟩ NWs. The bulk equilibrium length in the ⟨110⟩ direction is 3.87 Å and in the ⟨111⟩ direction is 9.47 Å. The increase in equilibrium axial lattice constant with smaller size is more significant for ⟨110⟩ NWs, while the Young's modulus softening is more significant for ⟨111⟩ NWs.

In order to understand these effects, we investigated the surface properties of the low index surfaces relevant to ⟨110⟩ and ⟨111⟩ NWs. We calculated the surface energies, surface stresses, and surface elasticity moduli for the {100} symmetric dihydride and the {111} and {110} surfaces. The {100} symmetric dihydride and the {111} surfaces form the facets of the ⟨111⟩ NWs and the {110} surfaces form the facets of the ⟨110⟩ NW. We use the definitions of surface energy, surface stress, and surface elasticity moduli as defined in Ref. 51. For the {100} surface, we use a 16 layer thick slab consisting of 16 Si atoms and 4 H atoms in a unit cell. The {110} surface consists of a 15 layer thick slab with 30 Si atoms and 4 H atoms in a unit cell, while the {111} surface consists of 12 layers of atoms with 24 Si atoms and 4 H atoms in a unit cell. The atomic positions were relaxed until the forces on each atom were less than <0.01 eV/Å. After the surface stresses and elasticity moduli were calculated in these minimal unit cell configurations, they were transformed to relevant crystal orientations using the appropriate tensor transformations. Index 1 is purposefully chosen to be along the NW orientation and index 2 along the orthogonal direction of the surface and index 1.

The surface energies γ, stress f_{IJ}, and elasticity moduli d_{IJ} of the {001}, {111}, and {110} Si surfaces are displayed in Table V. For the surface energies, we use the hydrogen chemical potential associated with the hydrogen molecule. We note that the {111} surface has the lowest surface energy and is the most preferred of the three. The surface stress is the first derivative of the surface energy with respect to strain per unit area. The surface stresses are negative, indicating that the surfaces are in a state of compression and have a tendency to elongate the lattice. The surface stresses for both the {111} and the {110} surfaces are small. However, the surface stress for the {001} surface is -0.230 eV/Å^2 in the ⟨110⟩ direction, which is the along the Si-H bond in the dihydride. The surface is in a larger compressive state in the direction of the dihydrides due to the H-H repulsion between neighboring H atoms, which cause a significant tendency to elongate the lattice along that direction. The compressive state of the various Si surfaces cause our NWs to elongate in the axial direction and, in particular, the large {001} surface stress explains why the ⟨110⟩ NWs have more significant elongation in its equilibrium lattice constant L_0 than ⟨111⟩ NWs. As the diameter of the Si NWs become smaller, the surface stress contribution increases, thus resulting in a larger equilibrium lattice constant with smaller diameter.

In addition, we calculated the surface elasticity moduli, which are the second order strain derivatives of surface energy with respect to strain per unit area. The elasticity constants d_{11}, d_{22}, d_{12}, and d_{44} are all negative, indicating a softening effect. The removal of the Si bonds in forming our surfaces softens the surface stiffness with respect to bulk Si. In particular, we were interested in the d_{11} component of these various surfaces which have been deliberately chosen to be along axes corresponding to the relevant NW direction. We note that while the elasticity moduli d_{11} were -0.485 eV/Å^2 and -0.431 eV/Å^2 for the {001} and {111} surfaces, respectively, it was -1.813 eV/Å^2 for the {110} surface. The {110} surface had a much stronger softening effect along the ⟨111⟩ direction than the {001} and {111} surfaces along the ⟨110⟩ direction. Young's modulus tends to soften more significantly for ⟨111⟩ NWs as its size decreases due to its {110} facets. We also note that the surface stress for the {001} surface was already converged within 0.1 eV/Å^2 for a four atom thick slab, while the elasticity constants tended to converge more slowly, supportive of the observa-

TABLE IV. Elastic constants and various Young's moduli and Poisson ratios for bulk Si from DFT simulations and literature.

	DFT with GGA	Expt.[a]
C_{11} (GPa)	154.6	165.7
C_{12} (GPa)	57.5	63.9
C_{44} (GPa)	75.3	79.6
$Y'_{\langle 110\rangle}$ (GPa)	159.4	169.1
$Y'_{\langle 111\rangle}$ (GPa)	176.6	187.9
$\nu'_{[110],[001]}$	0.35	0.35
$\nu'_{[110],[1\bar{1}1]}$	0.16	0.16
$\nu'_{[111],j}$	0.17	0.18

[a]Reference 50.

TABLE V. Surface energies γ, stresses f_{IJ}, and elasticity moduli d_{IJ} of {001}, {111}, and {110} surfaces (all values are given in units of eV/Å^2). The {001} and {110} surfaces are relevant for ⟨110⟩ NWs, and the {110} surface is relevant for ⟨111⟩ NWs. Index 1 is purposefully chosen to be along the NW orientation, and index 2 along the orthogonal direction of the surface and index 1. For the (001) surface, indices 1 and 2 correspond to [110] (along the direction of the dihydride bonds) and [1$\bar{1}$0]. For the (111) surface, [$\bar{1}$10] and [$\bar{1}\bar{1}$2] correspond to indices 1 and 2. For the (110) surface, we choose 1 and 2 to be [$\bar{1}$11] and [1$\bar{1}$2]. 4≡12 for expressing the elasticity tensor using Voigt notation.

Surface	γ	f_{11}	f_{22}	f_{12}	d_{11}	d_{22}	d_{12}	d_{44}	d_{14}	d_{24}
(001)	0.024	−0.230	−0.013	0	−0.485	−1.191	−1.455	−1.510	0	0
(111)	0.004	−0.002	−0.004	0	−0.431	−0.425	−0.437	−0.052	0	0
(110)	0.005	−0.004	−0.001	0.004	−1.813	−2.701	−1.035	−0.2136	−0.788	−0.467

tions that surface stress comes from the extrinsic H-H interactions and surface elasticity components come from intrinsic contributions.[52]

B. Electronic properties

In Table II, we show computed electronic properties, such as electron and hole effective masses $m_{e,h}$, conduction and valence band deformation potentials $\frac{\partial E_{c,v}}{\partial \varepsilon}$, band gap E_g, work function WF, and work function deformation potential $\frac{\partial \mathrm{WF}}{\partial \varepsilon}$. The band gap showed a usual decrease with increasing diameter. The differences in the band gap and effective mass for NWs of different orientations can be qualitatively understood from a simple effective mass picture as will be discussed in Sec. IV. Here, we point out that $E_g^{\langle 110\rangle} < E_g^{\langle 111\rangle}$ for the same diameter NWs. Also, $m_e^{\langle 110\rangle} < m_e^{\langle 111\rangle}$ and $m_h^{\langle 110\rangle} < m_h^{\langle 111\rangle}$. The WF was calculated by placing the Fermi level E_f at midgap, close to where it should lie for intrinsic semiconductors. The WF was mostly size independent for ⟨111⟩ NWs, while it tended to increase slightly for ⟨110⟩ NWs with decreasing diameter. The deformation potentials $\frac{\partial \mathrm{WF}}{\partial \varepsilon}$, $\frac{\partial E_c}{\partial \varepsilon}$, and $\frac{\partial E_v}{\partial \varepsilon}$ were calculated by linear fits to the conduction and valence band edges with strain. In Sec. IV we discuss the dependence of NW electronic properties on strain.

IV. EFFECT OF STRAIN ON ELECTRONIC PROPERTIES

A. Electronic band structure of Si nanowires

The eight different NWs were strained up to a range of 10% compressive and tensile strain in 1% increments. The strain is defined with respect to the equilibrium axial spacing of that particular NW, and not bulk Si. As discussed above, due to size effects, NWs have some built-in axial strain with respect to bulk Si due to surface effects.

The main changes to the band structure of Si NWs are shown in Fig. 2, where we show the band structure of the (a) ⟨110⟩ and (b) ⟨111⟩ NWs (numbers 3 and 8) about 2 nm in diameter under axial tensile and compressive strain. We start with a discussion of the band structure of these unstrained NWs. The general features of the conduction bands can be understood from effective mass theory and the band structure of bulk Si. The conduction band edge of bulk Si consists of six equivalent anisotropic Δ valleys, located at about 0.85

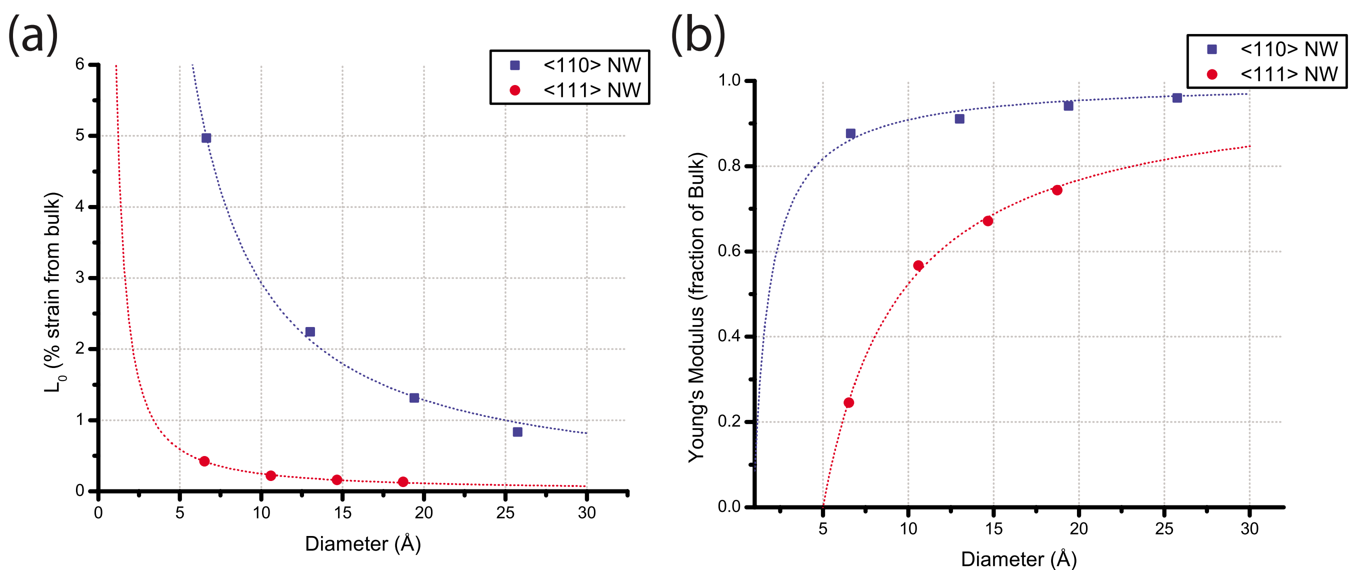

FIG. 2. (Color online) Plot of (a) equilibrium axial lattice constant L_0 (% strain from bulk) and (b) Young's modulus Y (fraction of bulk Young's modulus) versus diameter d (Å). The equilibrium axial lattice constant was fit by the curve $C_1/d + C_2/d^2$, and Young's modulus was fit by $1 - D_1/d - D_2/d^2$.

TABLE VI. Projections of various states.

State	$\|s\rangle$	$\|p_X\rangle$	$\|p_Y\rangle$	$\|p_Z\rangle$
Δ_2	0.6903	0	0.6136	0.3835
c_1	0.8085	0.1617	0.5659	0
Δ_4	0.8607	0.4303	0.0861	0.2582
v_1	0.0994	0	0.0497	0.9938
v_2	0.2570	0.0642	0.9637	0.0321
Δ_6	0.8874	0.2662	0.2662	0.2662
v_3	0.0524	0.0524	0.0524	0.9959
v_4	0.1686	0.9837	0.0562	0.0281

$\times 2\pi/a$ along the $\pm[100]$, $\pm[010]$, and $\pm[001]$ directions. Further in the text, we refer to the six valleys as $[\pm a,0,0]$, $[0,\pm a,0]$, and $[0,0,\pm a]$. The valleys are ellipsoids with transverse mass m_t=0.19m_0 and longitudinal mass m_l=0.98m_0.

For the $\langle 110\rangle$ NW, the conduction band minimum at Γ is formed from the two Δ valleys $[0,0,\pm a]$ of bulk Si and is thus labeled Δ_2. Another minimum Δ_4 is formed from the bulk Si valleys at $[\pm a,0,0]$ and $[0,\pm a,0]$ and folded close to $\pm 0.5\frac{\pi}{a}$. According to this effective mass picture, $\langle 110\rangle$ wires with reasonably circular cross sections (no high aspect ratio) should be direct band gap.[53] Indeed, the conduction minimum Δ_2 at the Γ point has lower confinement energy than the conduction band minimum Δ_4. This is because the energy of Δ_2 is determined by the large longitudinal mass and smaller transverse mass in the confinement directions, while the energy of Δ_4 is determined by the smaller transverse mass. Similar analysis can be applied to NWs grown in other directions. Thus, the conduction band minimum of $\langle 111\rangle$ NWs are formed from the Δ valleys $[\pm a,0,0]$, $[0,\pm a,0]$, and $[0,0,\pm a]$ of bulk Si and labeled Δ_6. The minimum is located away from the Γ point and the wire is, in general, indirect band gap. The large effective mass in the growth direction results in a conduction band which is very flat. The conduction band is also very sensitive to the mor-

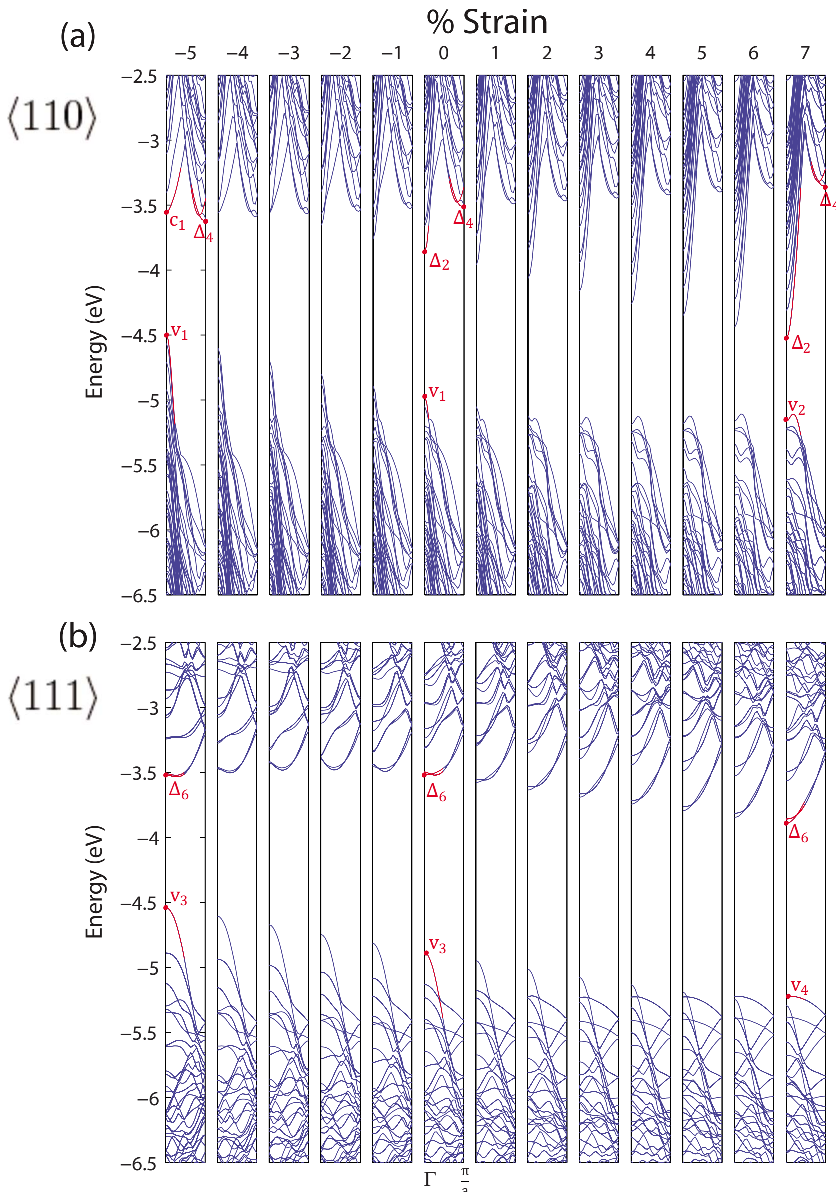

FIG. 3. (Color online) Band structure for (a) $\langle 110\rangle$ and (b) $\langle 111\rangle$ NWs about 2 nm in size (wires 3 and 8) under different amounts of strain.

phology of the NW, and the deviation of wire cross section from circular geometry lifts the degeneracy of the Δ_6 minimum. At last, the valence band maxima of the ⟨110⟩ and ⟨111⟩ NWs, positioned near the Γ point, are similar to those of bulk Si. There is, however, a significant mixing and splitting of the valence band, which cannot be explained by effective mass theory.

When the ⟨110⟩ NW is compressed, the energy of Δ_2 increases and eventually exceeds the energy of the Δ_4 state. We will refer to this transition as a direct-to-indirect band gap transition. Under tensile strain, the Δ_2 state is pulled down together with a subset of higher sub-bands at the Γ point. Remarkably, Δ_4 and another energetically close state at Γ, which we call c_1, remain fairly constant under tension or compression. At a tensile strain of 7%, the c_1 state is the 14th sub-band at Γ, while it is the lowest and the 2nd lowest at a strain of −7% and 0%, respectively. We note that the situation is somewhat different in bulk Si under uniaxial tensile stress in the ⟨110⟩ direction: while the splitting of Δ_2 and Δ_4 has the same sign, it is the Δ_4 valleys that are raised, while Δ_2 valleys are less affected. The valence band edge of ⟨110⟩ NWs is determined by the states v_1 and v_2. The v_1 state is the highest at zero strain and is shifted significantly with strain, rising under compression and falling under tension, while the v_2 state remains fairly constant. Therefore, under the tensile strain, when the v_1 state is pulled down, the NW becomes indirect band gap and the hole properties are determined by the v_2 state.

Applying strain to the ⟨111⟩ NW tended to lower the energy of Δ_6 under tension and raise it slightly under compression. As expected in the effective mass picture, there is no splitting of the conduction band minimum because all valleys are affected equally by strain. Consequently, the conduction band behavior under strain in ⟨111⟩ Si NWs is analogous to that of bulk Si under uniaxial strain in the ⟨111⟩ direction. The valence band behavior of ⟨111⟩ NWs is very similar to that of ⟨110⟩ NWs: the valence band state v_3 was raised under compression and lowered under tension, while v_4 remained fairly constant under strain. The lowering of the v_3 state below the v_4 state occurs at much larger tensile strain than the direct-to-indirect band gap transition (v_1 below the v_2) in the ⟨110⟩ NW.

The dramatic difference between the strain dependence of various states suggests that their wave functions have different symmetries. To check this prediction, in Table VI we show the projections of the wave functions of various states on s, p_X, p_Y, and p_Z states, where the Z axis is aligned with the axis of the NW. The projection of wave functions is done onto spherical harmonics that are within spheres of radius 1.3 Å around each Si atom. The character of each conduction and valence band edge state can also be seen in Fig. 4, which shows a corresponding charge density. As can be seen from Table VI, the v_1 state has a substantial s and p_Z character, while the v_2 is primarily of s and p_Y type. The same trend is seen for the v_3 and v_4 states of the ⟨111⟩ NW. This observation suggests that that the states that are extended along the axis of the wire are more susceptible to strain, while the states that are more localized are not. For conduction band edge states in ⟨110⟩ NWs, Δ_2 has a substantial p_Y and p_Z character, while Δ_4 has a substantial p_X and p_Z character. Δ_2 changes more with strain due to its p_Z character. Δ_4 does not shift as significantly with strain because its p_Z character is less and it has a strong p_Y component, which along with the larger Poisson ratio in this direction ($\nu_{[110],[001]}$, as shown in Table III) causes the state to shift upward slightly.

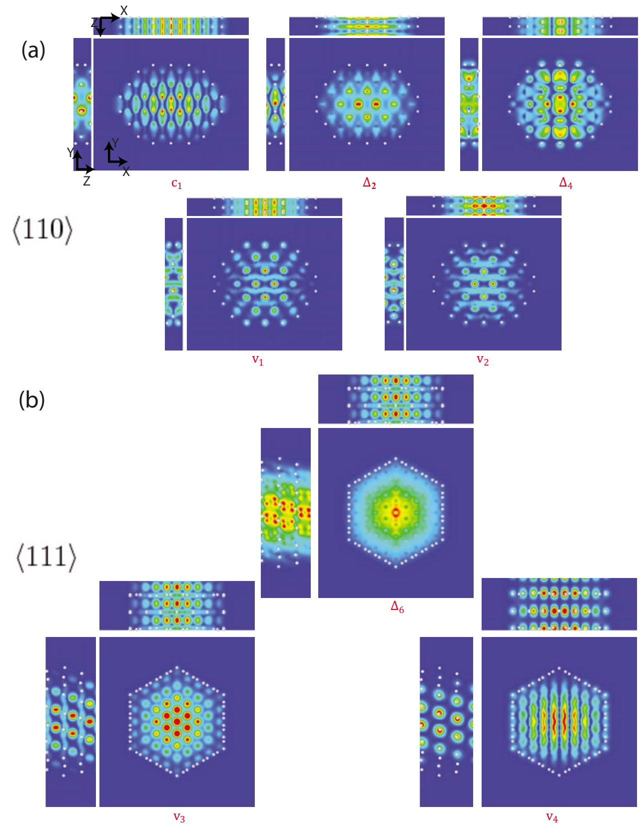

FIG. 4. (Color online) Electronic charge density of the conduction and valence band edge states for (a) the ⟨110⟩ NW and (b) the ⟨111⟩ NW. The states are labeled as in Fig. 3. The XY plane (middle), YZ plane (left), and XZ plane (top) are shown for each state where the charge is averaged along the out of plane axis. High density is indicated as red and low density is indicated as blue. The H atoms are also shown in the plots to give an idea of where the electronic charge is present spatially in the NW.

B. Band gaps of Si nanowires

The Si NW band gap variation with strain is shown in Fig. 5. The GGA bulk band gap of Si is 0.6 eV. While DFT within the local density approximation is known to underestimate band gap, more accurate quantum Monte Carlo calculations have shown that DFT reproduces the general trends of band gap change.[54] The behavior of the band gap is a direct consequence of the change in band structure described above. At zero strain, ⟨111⟩ wires tend to have a larger band gap than ⟨110⟩ wires of the same size due to smaller bulk Si effective masses in the confinement directions. This trend continues to hold in strained wires. In ⟨110⟩ NWs, compressive strain tended to first increase the band gap, due to rising of the Δ_2 state. However, the band gap increase is followed by a decrease, due to the v_1 state rising, while the bottom of conduction band Δ_4 remains fairly constant. Tensile strain causes

a monotonous closing of the band gap, due to lowering of the Δ_2 state, while the top of the valence band v_2 remains constant. In strained ⟨111⟩ NWs, the bottom of the conduction band Δ_6 remains almost nearly constant. Thus, compressive strain tended to decrease the band gap, due to rising of the v_3 state, while tensile strain tends to keep the band gap constant, as the energies of Δ_6 and v_4 do not change significantly.

In the NWs considered, the change in the band gap is several tenths of electron volts with a few percent of strain, which is about an order of magnitude lower than a band gap change in bulk Si for the same amount of strain. We note that band gap variation with strain tends to be more significant for larger diameter NWs, while the band gap of smaller diameter NWs remains fairly constant under tensile or compressive strain. We would expect that as the diameter increases, the role of strain would also increase, reaching the limit of bulk Si.

C. Effective masses of Si nanowires

The effective masses $m^*=\hbar^2(\frac{\partial^2 E}{\partial^2 k})^{-1}$ of the various wires are determined by performing a second derivative fit to the bottom of the conduction band and top of the valence band, where we have used 40 k points along the axis of the NW. The bulk Si effective masses of our simulations in the ⟨110⟩ direction are $m_e=0.28m_0$, $m_{hh}=2.56m_0$, $m_{lh}=0.13m_0$, and $m_{so}=0.29m_0$ (note that we do not include spin orbit coupling in our calculations). The bulk Si effective masses of our simulations in the ⟨111⟩ direction are $m_e=1.81m_0$, $m_{hh}=0.71m_0$, $m_{lh}=0.11m_0$, and $m_{so}=0.71m_0$.

Figure 6 shows the variation of the electron and hole effective masses in the lowest sub-band with strain. In Fig. 6(a), the ⟨110⟩ NW shows a trend which is qualitatively similar to that in bulk Si: the effective mass is determined by the Δ_2 state under tension and by the Δ_4 and c_1 states under compression. Note that, unlike in the case of bulk Si, quantum confinement already split the Δ_2 and Δ_4 states even at zero strain. One may draw an analogy between quantum confinement and a built-in tensile strain, which splits the Δ_2 and Δ_4 states and decreases transport effective mass. Therefore, under tension, electron effective mass shows only a slight increase due to a change in curvature of the Δ_2 state. However, under compressive strain, effective mass shows a jump, associated with a direct-to-indirect band gap transition as Δ_2 rises above the c_1 and Δ_4 states. This happens at −7%, −4%, −3%, and −3%, when the electron effective mass increases by factors of 7.1, 6.4, 5.6, and 3.7 for wires 1, 2, 3, and 4, respectively. The strain dependence of transport effective mass in ⟨110⟩ NWs is qualitatively similar to that in bulk Si under strain in the ⟨110⟩ direction. However, a present quantum confinement has already caused a splitting of the Δ_2 and Δ_4 states and, therefore, there is no further benefit in tensile strain. We note that the effective mass is already below a value of $m_t=0.19$ at zero strain, which suggests that further improvement by tensile strain will not be significant. We do not show the electron effective mass of ⟨111⟩ Si NWs. Similar to the case of bulk Si under strain in the ⟨111⟩ direction, there is no splitting of the triply degenerate conduction band of ⟨111⟩ Si NWs because all states are affected equally by strain. The conduction bands are flat and sensitive to changes in the morphology of the NW. The ⟨111⟩ NWs generally have an electron effective mass between m_0 and $3m_0$ under different amounts of strain.

In Fig. 6(b) the hole effective mass is shown as a function of strain. For ⟨110⟩ NWs, the hole effective mass shows an insignificant decrease under compressive strain. However, under tensile strain of 9.5%, 4%, 3%, and 2%, the valence band undergoes a direct-to-indirect transition, as the v_1 state falls below the v_2 state, for wires 1, 2, 3, and 4, respectively. The hole effective mass jumps by factors of 7.9, 2.7, 2.9, and 3, respectively, for these cases. The situation is opposite to the case of the conduction band: the transport effective mass does not change significantly under compression and shows

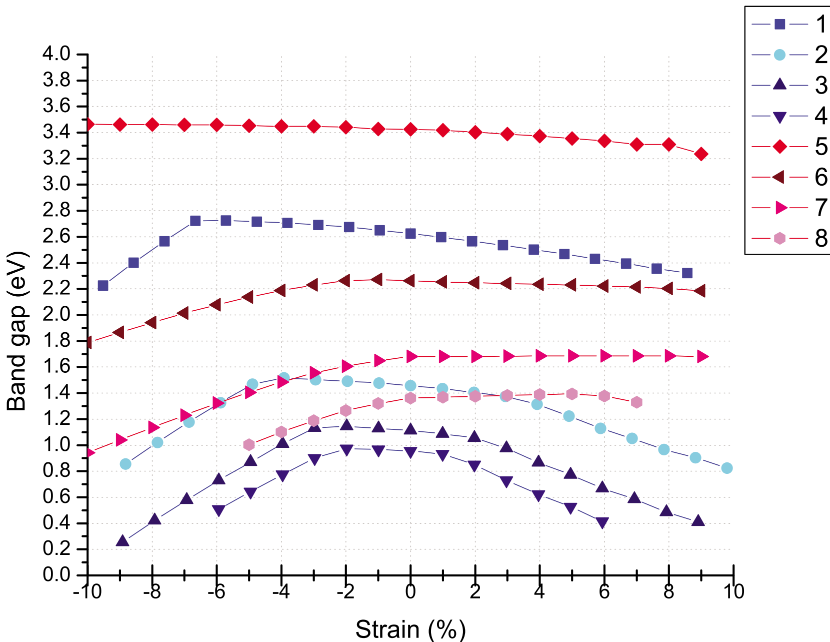

FIG. 5. (Color online) Band gap versus strain for ⟨110⟩ and ⟨111⟩ Si NWs of different sizes.

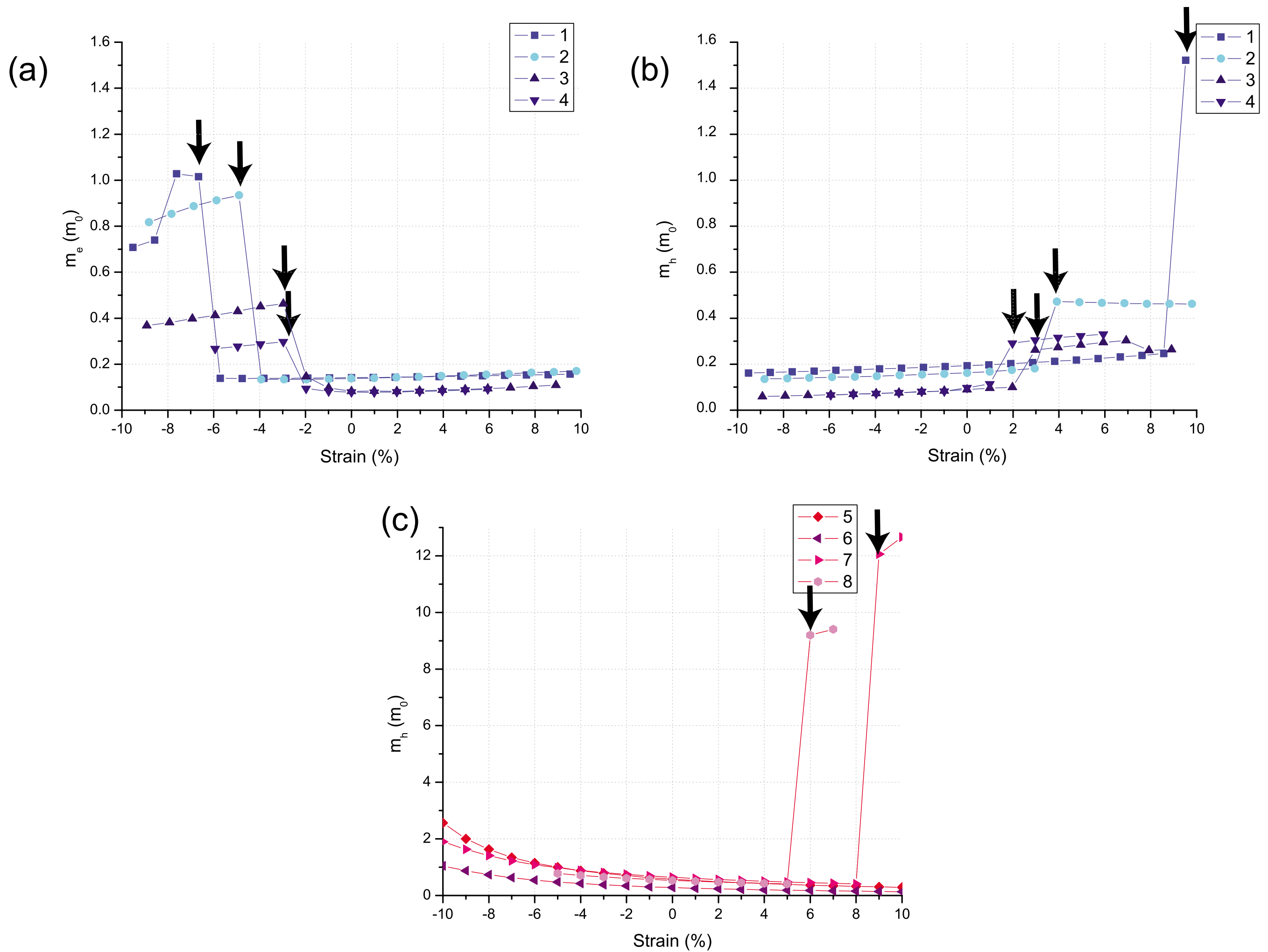

FIG. 6. (Color online) Electron and hole effective masses versus strain of Si NWs. (a) shows the electron effective mass versus strain of ⟨110⟩ Si NWs of different sizes. The ⟨110⟩ NWs undergo a direct-to-indirect band gap transition under compressive strain along with an associated jump in the electron effective mass. This happens at −7%, −4%, −3%, and −3% for wires 1, 2, 3, and 4 respectively. (b) shows the hole effective mass versus strain of ⟨110⟩ Si NWs of different sizes. The valence bands also undergo a Γ to non-Γ transition under tensile strain at 10%, 4%, 3%, and 2% for wires 1, 2, 3, and 4 respectively. (c) shows the hole effective mass versus strain of ⟨111⟩ Si NWs of different sizes. The ⟨111⟩ Si NWs valence edge state also transitions away from Γ at 9% and 6% tensile strain for NWs 7 and 8, respectively.

a strong increase under tension. The hole effective mass dependence on strain in ⟨111⟩ NWs, shown in Fig. 6(c), shows a slight decrease under tension up until the strain, at which the states v_3 and v_4 are aligned. When the v_3 state is pulled below the v_4 state, the effective mass jumps by a factor of ~10 for all NWs. The jump occurs at strain of 9% and 6% for NWs 7 and 8, respectively, which is significantly higher than the similar jump in ⟨110⟩ NWs. Under compressive strain, the hole effective mass shows a strong monotonous increase, due to a change in the parabolicity of the v_3 state.

Based on the behavior of the effective mass alone, we can conclude that the electron mobility in ⟨110⟩ NWs will decrease slightly under tension and degrade by a factor of 3–7 under compression. Also, experimentally, one may expect a nonmonotonic behavior of electron mobility with strain in ⟨111⟩ NWs. The hole mobility in ⟨110⟩ Si NWs is likely to deteriorate by a factor of 3–8 under tension and improve slightly under compression. Finally, in ⟨111⟩ Si NWs, the hole mobility is likely to deteriorate steadily under compression and improve under tension. Under very high tensile strain, the hole mobility must decrease rapidly due to a jump of the hole effective mass. The conclusion on the mobility behavior drawn here is not final, as it does not account for a change in deformation potentials. We will revisit the mobility behavior in Sec. IV D and IV E.

D. Deformation potential of Si nanowires

Electron and hole deformation potentials $\frac{\partial E_c}{\partial \varepsilon}$ and $\frac{\partial E_v}{\partial \varepsilon}$ are shown in Table II for unstrained NWs. The value of the deformation potential gives the rate at which lowest conduction or highest valence sub-bands change with strain and is in direct relation to the band structure. Thus, the electron deformation potential of ⟨110⟩ NWs is a factor of 3.3 higher than that of ⟨111⟩ NWs for the smallest diameter and about a factor of 1.88 for the largest diameter. This difference is due to a larger sensitivity to strain of the Δ_2 states in ⟨110⟩ NWs over the Δ_6 states in ⟨111⟩ NWs. We note that, while electron

TABLE VII. Deformation potentials calculated from DFT on bulk Si. All quantities in eV.

	DFT result	Literature[a]
Ξ_u	8.81	10.5
b	−3.50	−2.33
d	−4.43	−4.75
$\Xi_d+\frac{\Xi_u}{3}-a$	2.93	2.5
Ξ_d	−2.3	2.1
a	−2.4	1.2

[a]Reference 8.

deformation potential is smaller by a factor of ~2–3 for ⟨111⟩ NWs, the effective mass is larger by a factor of ~7–12. Therefore, the electron mobility, inversely proportional to the effective mass and a square of deformation potential, should not differ significantly as these two factors compensate each other. Hole deformation potentials are also larger for ⟨110⟩ NWs: the difference varies from a factor of 1.9 for the smallest diameter to 1.3 for the largest diameter.

For a comparison with bulk deformation potentials, we have calculated the deformation potentials of bulk Si using DFT. The formulas providing the quantitative shifts in energies and splitting as a function of the uniaxial deformation potentials b, d, and Ξ_u, and the dilatation deformation potentials a and Ξ_d are found in Ref. 55. Using the strain $\epsilon_1=\delta$, we obtain b, Ξ_u, and $\Xi_d+\frac{\Xi_d}{3}-a$. Next, using the strain $\epsilon_4=2\delta$, we obtain d. The uniaxial deformation potentials we calculate agree fairly well with that in the literature. On the other hand, the dilatation deformation potentials a and Ξ_d are difficult to measure or calculate due to the need for an absolute energy reference. A number of values have been reported in the literature for Ξ_d.[56] In order to determine Ξ_d, we used a 30 slab {100} Si Surface with 60 Si atoms and 8 H atoms. The atoms were not relaxed and strained with $\epsilon_1=\delta$. The vacuum level of the slab was used as an absolute reference energy. Using our calculations, we obtained Ξ_d and then we used our above result for $\Xi_d+\frac{\Xi_d}{3}-a$ to obtain a.

The results are compiled in Table VII. We note that the uniaxial deformation potentials Ξ_u, b, and d agree well with experimental reports. We have used the deformation potentials reported in Ref. 8 to calculate the expected change in deformation potentials along the particular NW directions. For bulk Si in the ⟨110⟩ direction under uniaxial stress, the change in conduction bands are $\frac{\partial E_c^{\Delta_2}}{\partial e}=-2.4$ eV and $\frac{\partial E_c^{\Delta_4}}{\partial e}=6.2$ eV; $\frac{\partial E_v}{\partial e}=0.7\pm 3.2$ eV. For bulk Si in the ⟨111⟩ direction, $\frac{\partial E_c^{\Delta_6}}{\partial e}=3.7$ eV and $\frac{\partial E_v}{\partial e}=0.8\pm 3.2$ eV. There are notable differences between the shifts in conduction and valence band edge states in bulk Si versus Si NWs, most notably that the deformation potentials in Si NWs are shifted to be more negative. The main difference is that our structures are one-dimensional (1D) as opposed to three-dimensional (3D). In Si NWs, we only have a 1D density of states so that tensile strain will shift all bands downward as the states move closer together and the Fermi level is lowered. In bulk Si, there is a 3D density of states, so that while uniaxial tensile stress will still move the states closer together in direction of the stress, the states in the orthogonal directions will spread further apart with the Poisson ratio; thus, the Fermi level will not necessarily be lowered.

As discussed above, under compressive strain in ⟨110⟩ NWs, a transition occurred at which the Δ_2 state is pulled up and the lowest conduction sub-bands are determined by the Δ_4 and c_1 states. An immediate consequence of this transition is a dramatic decrease in deformation potential because these states are much less sensitive to strain than the Δ_2 state. For example, in NW 3, this results in a decrease in the absolute value of the electron deformation potential from 10.3 eV, at zero strain, to 2.3 eV under compressive strain, i.e., a 20-fold decrease in the squared value. The qualitative trend is the same for all other ⟨110⟩ NWs. As expected from the discussion of the band structure, ⟨111⟩ NWs do not show any change in electron deformation potential because the Δ_6 states are not affected significantly. A qualitatively similar but quantitatively much larger reduction in the hole deformation potential can be observed for both growth orientations under tensile strain. The ⟨110⟩ NW 3 shows a decrease in magnitude from 8.1 to 0.9 eV, while the ⟨111⟩ NW 8 shows a decrease from 6.6 to 0.2 eV. The decrease in the squared values are ~81 and ~1000 times, respectively.

We now revisit the discussion on the effects of strain on mobility. For the case of electron mobility in ⟨110⟩ NWs, we observe a counterplay between deformation potentials and the effective mass of the lowest sub-band: as the deformation potential decreases, the effective mass increases and vice versa. Quantitative comparison using Eq. (1) suggests that even with a concurrent three- to sevenfold increase in the effective mass, the electron mobility in ⟨110⟩ NWs must display a two- to sixfold increase under compressive strain when a direct-to-indirect band gap transition occurs (at about 3% strain for NW 3). The effect is similar for the ⟨110⟩ NW hole mobilities except that mobility improvement should occur at tensile strain. Based on the decrease in the deformation potential and a concurrent increase in the effective mass, the hole mobility must increase 10–30 times in ⟨110⟩ NWs under tensile strain when a direct-to-indirect band gap transition occurs (at about 3% strain for NW 3).

In ⟨111⟩ NWs, the electron mobility should not change significantly under tensile or compressive strain, as the conduction band of ⟨111⟩ NWs is fairly immune to strain. Finally, the hole mobility in ⟨111⟩ NWs in must show a slight steady decrease under compression and increase under tension due to the changes in the hole effective mass alone. However, at very high tensile strain of 6%, when a transition from the v_3 to v_4 state occurs, the hole mobility must show an ~100-fold increase. Note that detailed calculations of scattering rates are required in order to give a more precise prediction.

E. Work functions of Si nanowires

The Si NW WF is an important physical quantity in understanding NW field emission.[57] The WF dictates the direction of charge transfer and influences the selectivity of molecules as chemical sensors.[58] It also affects the band lineup at

the NW/metal contact interface and can impact device performance. The WF can be measured experimentally using a Kelvin probe force microscope or electron emission based methods. WF is defined as $WF=\phi-E_f$, where ϕ is the vacuum level and E_f is the Fermi level of the system. For Si NWs, we placed the E_f at midgap, close to where it should lie for intrinsic semiconductors. The vacuum level ϕ was determined from the average potential in the vacuum region where the potential approaches a constant.

Figure 7(a) displays the WF change of the eight NWs under different amounts of strain. The WF of the Si NWs was mostly size independent for ⟨111⟩ NWs, while it tended to increase slightly for ⟨110⟩ NWs with decreasing diameter. We also calculated the change in WF with strain $\frac{\partial(WF)}{\partial\varepsilon}$ and note that strain had a larger effect on ⟨110⟩ NWs. We performed calculations on Si slabs for comparison. We performed convergence tests on the number of layers and on the vacuum space so that the WF of these slabs converged within 0.01 eV. We examined the three low index surfaces, {111}, {100}, and {110}. The WF for the three crystallographic faces were 4.27, 4.19, and 4.27 eV for the {111}, {100}, and {110} surfaces, respectively.

The WF increase (decrease) can be due to an enhanced (reduced) dipole or a lowering (rising) of its intrinsic bulk Fermi energy.[59] We quantitatively evaluate these two contributions by rewriting WF as

$$WF=\phi-E_f=(\phi-V_{\mathrm{ref}})-(E_f-V_{\mathrm{ref}}), \tag{3}$$

where V_{ref} is the average electrostatic potential at the core of the Si atoms in the NW. The first term is this potential with respect to the vacuum level ϕ, and its change reflects a change in surface dipole contribution. The second term describes how the Fermi energy E_f is above the average potential and is related to material's intrinsic bulk electronic structure. Figure 7(b) displays the average electrostatic potential at the Si atomic core, $V_{\mathrm{ref}}-\phi$, with strain. The average Si atom potential increased slightly with decreasing diameter for ⟨110⟩ NWs, while it stayed about the same for ⟨111⟩ NWs. This indicates that the slight increase in the WF of ⟨110⟩ NWs with decreasing diameter comes about from surface dipole effects. More significant is the change in surface dipole contribution due to strain. The average Si atom potential increases under tensile strain as less electronic charge is distributed on the H atoms. Under compression, more charge is shifted onto the H atoms, resulting in a larger dipole and lowering the potential within the NW. Figure 7(c) illustrates the change in charge density of the ⟨110⟩ NW 3 with 1% axial tensile strain versus equilibrium length. Red, orange, and yellow indicate positive charge transfer, while green, indigo, blue, and purple indicate negative charge transfer. The charge transfer plot indicates that charge has transferred from surface H bonds onto the interior of the NW with tensile strain decreasing the strength of the dipole. The WF is lowered due to surface effects with tensile strain. However, a stronger contribution to the WF comes from the second term E_f-V_{ref} in Eq. (3). This term decreases more rapidly than the potential raising from the surface dipoles under tensile strain and, thus, the overall trend in WF is to increase under tensile strain. As the NW is stretched with axial tension, the density of states in k space increases and, thus, the Fermi energy decreases.

V. SUMMARY

In conclusion, we have studied the mechanical properties of low diameter Si NWs and the effects of axial strain on their electronic properties. We evaluated the Young's modulus, Poisson ratio, band gap, effective mass, deformation potential, and work function for ⟨110⟩ and ⟨111⟩ NWs from 0.7 to 2.6 nm in diameter. Our calculations show that Young's modulus tended to decrease with smaller diameter due to an increasing contribution of the surface. The equilibrium lattice constant increased in size with smaller diameter NWs as the surface tends to provide a tensile stress to the NWs. In studying the electronic properties, it was noted that $E_g^{\langle 110\rangle}<E_g^{\langle 111\rangle}$ for the same diameter NWs and $m_e^{\langle 110\rangle}<m_e^{\langle 111\rangle}$ and $m_h^{\langle 110\rangle}<m_h^{\langle 111\rangle}$. We also studied the effects of strain on the NW band structure in the range from 10% compressive to 10% tensile strain in 1% increments.

An important finding we report in this paper is the possibility for achieving a many fold increase in electron and hole mobilities of Si NWs under strain. In all cases, the increase is caused by a dramatic decrease in deformation potential, when a direct-to-indirect band gap transition occurs and the conduction or valence band is determined by strain-insensitive states. The effect is much stronger than a decrease in mobility contributed by a concurrent increase in the effective mass. In ⟨110⟩ Si NWs, a two- to sixfold electron mobility increase is expected under compressive strain. We note that the expected trend of mobility with strain is opposite to that in bulk Si or large diameter NWs, where the tensile strain in the ⟨110⟩ direction would increase electron mobility. The hole mobility is expected to increase by 10–30 times in ⟨110⟩ Si NWs and by ~100 times in ⟨111⟩ Si NWs under tensile strain. More detailed calculations of full band scattering rates would be needed to get a more precise estimate. The main difference between our small diameter Si NWs and larger diameter NWs or bulk Si is the presence of quantum confinement, which acts similarly to strain and splits the degeneracy of the bulk conduction and valence band edge states.

It was also found that the band gap of Si NWs can be modified by a few tenths of an eV with a few percent strain. The qualitative behavior of the conduction band of Si NW is similar to that of bulk Si, where equivalent valleys can be energetically split by uniaxial strain. However, in NWs the spitting due to strain is preceded by that due to quantum confinement. In ⟨110⟩ NWs, where electron effective mass is below $m_t=0.19m_0$ in unstrained NW, tensile strain does not decrease electron effective mass any further. In ⟨111⟩ NWs, the degeneracy of the lowest conduction sub-band remains largely unaffected by strain or confinement. The analysis of the valence band shows that the hole effective mass tends to

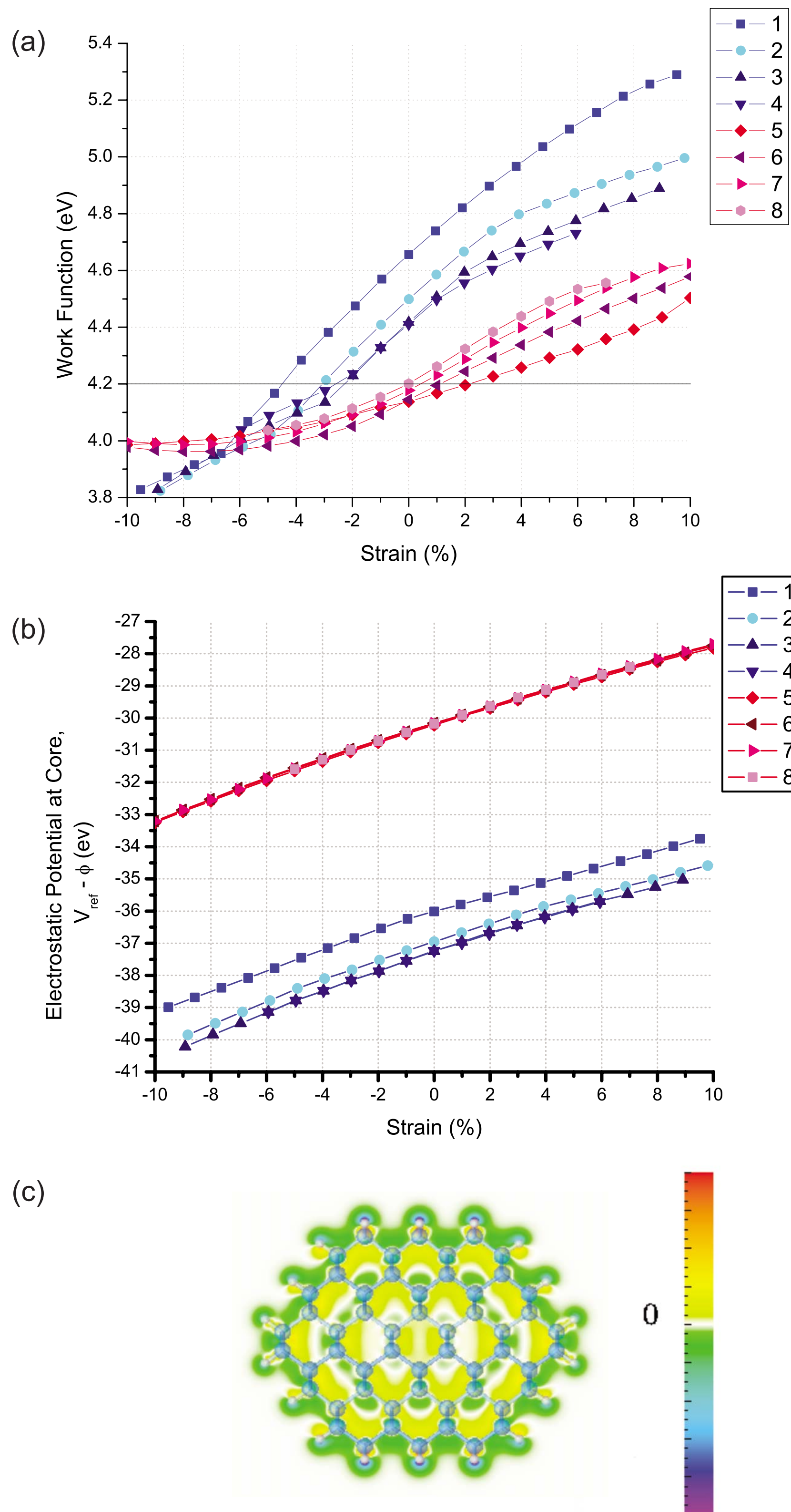

FIG. 7. (Color online) WF versus strain data and analysis for NWs. (a) displays the WF versus strain for ⟨110⟩ and ⟨111⟩ Si NWs of different sizes. The bulk Si WF of 4.2 eV is also plotted for comparison. (b) and (c) give a quantitative analysis of the surface dipole contribution to WF change in Si NWs. (b) displays the change in average Si atom potential with respect to vacuum, $V_{\mathrm{ref}}-\phi$, plotted as a function of strain. (c) shows the change in charge density of NW 3 after 1% tensile strain. Red, orange, and yellow indicate positive charge transfer, while green, blue, indigo, and purple indicate negative charge transfer. The figure shows that dipole is reduced with increasing tension, which signifies the increase in V_{ref} in (b).

increase under compression and decrease under tension. Finally, we also studied the WF of these NWs and found that we can increase (decrease) the WF of NWs with tensile (compressive) strain. The change in WF comes about primarily from the change in electron density with strain. We have explored strain as a method to engineer the electronic properties of Si NWs and how it can be used to enhance or diminish the effects of quantum confinement.

ACKNOWLEDGMENTS

The authors would like to thank the San Diego Supercomputer Center for computational resources and the Stanford Nanowire Facility for helpful discussions. P.W.L. would like to thank Stanford and NSF. The authors would also like to thank the NSF Center of Integrated Nanomechanical Systems (COINS) for financial support.

*pleu@stanford.edu
†Also at Silvaco Data Systems, Inc., Santa Clara, CA 95054; alexeis@silvaco.com
‡Also at University of Texas at Dallas, Richardson, TX 75083; kyeongjae.cho@utdallas.edu
[1] X. Y. Zhao, C. M. Wei, L. Yang, and M. Y. Chou, Phys. Rev. Lett. **92**, 236805 (2004).
[2] T. Vo, A. J. Williamson, and G. Galli, Phys. Rev. B **74**, 045116 (2006).
[3] J. A. Yan, L. Yang, and M. Y. Chou, Phys. Rev. B **76**, 115319(2007).
[4] P. W. Leu, B. Shan, and K. Cho, Phys. Rev. B **73**, 195320 (2006).
[5] A. Svizhenko, P. W. Leu, and K. Cho, Phys. Rev. B **75**, 125417 (2007).
[6] Y. J. Ko, M. Shin, S. Lee, and K. W. Park, J. Appl. Phys. **89**, 374 (2001).
[7] A. K. Singh, V. Kumar, R. Note, and Y. Kawazoe, Nano Lett. **6**, 920 (2006).
[8] M. V. Fischetti and S. E. Laux, J. Appl. Phys. **80**, 2234(1996).
[9] M. Luisier, A. Schenk, W. Fichtner, and G. Klimeck, Phys. Rev. B **74**, 205323 (2006).
[10] F. Bogar, J. W. Mintmire, F. Bartha, T. Mezo, and C. VanAlsenoy, Phys. Rev. B **72**, 085452 (2005).
[11] R. Heyd, A. Charlier, and E. McRae, Phys. Rev. B **55**, 6820 (1997).
[12] C. J. Park, Y. H. Kim, and K. J. Chang, Phys. Rev. B **60**, 10656(1999).
[13] M. Verissimo-Alves, B. Koiller, H. Chacham, and R. B. Capaz, Phys. Rev. B **67**, 161401(R) (2003).
[14] S. Peng and K. Cho, Trans. ASME, J. Appl. Mech. **69**, 451 (2002).
[15] K. H. Hong, J. Kim, S.-H. Lee, and J. Shin, Nano Lett. **8**, 1335 (2008).
[16] D. M. Lyons, R. M. Ryan, M. A. Morris, and J. D. Holmes, Nano Lett. **2**, 811 (2002).
[17] G. Audoit, T. N. Mhuircheartaigh, S. M. Lipson, M. A. Morris, W. J. Blau, and J. D. Holmes, J. Mater. Chem. **15**, 4809 (2005).
[18] H. W. Seo, S. Y. Bae, J. Park, H. N. Yang, K. S. Park, and S. Kim, J. Chem. Phys. **116**, 9492 (2002).
[19] R. He and P. Yang, Nat. Nanotechnol. **1**, 42 (2006).
[20] B. M. Haugerud, L. A. Bosworth, and R. E. Belford, J. Appl. Phys. **94**, 4102 (2003).
[21] H. R. Gutierrez, R. Magalhaes-Paniago, J. R. R. Bortoleto, and M. A. Cotta, Appl. Phys. Lett. **85**, 3581 (2004).
[22] J. L. Taraci, M. J. Hytch, T. Clement, P. Peralta, M. R. McCartney, J. Drucker, and S. T. Picraux, Nanotechnology **16**, 2365 (2005).
[23] M. W. Larsson, J. B. Wagner, M. Wallin, P. Hakansson, L. E. Froberg, L. Samuelson, and L. R. Wallenberg, Nanotechnology **18**, 015504 (2007).
[24] J. M. Garcia, L. Gonzalez, M. U. Gonzalez, J. P. Silveira, Y. Gonzalez, and F. Briones, J. Cryst. Growth **227-228**, 975 (2001).
[25] L. T. Ngo, D. Almecija, J. E. Sader, B. Daly, N. Petkov, J. D. Holmes, D. Erts, and J. J. Boland, Nano Lett. **6**, 2964 (2006).
[26] S. Hoffmann, I. Utke, B. Moser, J. Michler, S. H. Christiansen, V. Schmidt, S. Senz, P. Werner, U. Gosele, and C. Ballif, Nano Lett. **6**, 622 (2006).
[27] T. Kizuka, Y. Takatani, K. Asaka, and R. Yoshizaki, Phys. Rev. B **72**, 035333 (2005).
[28] M. Menon, D. Srivastava, I. Ponomareva, and L. A. Chernozatonskii, Phys. Rev. B **70**, 125313 (2004).
[29] A. M. Morales and C. M. Lieber, Science **279**, 208 (1998).
[30] D. B. Kao, J. P. McVittie, W. D. Nix, and K. C. Saraswat, IEEE Trans. Electron Devices **35**, 25 (1988).
[31] H. Ohta, T. Watanabe, and I. Ohdomari, Jpn. J. Appl. Phys., Part 1 **46**, 3277(2007).
[32] M. Uematsu, H. Kageshima, K. Shiraishi, M. Nagase, S. Horiguchi, and Y. Takahashi, Solid-State Electron. **48**, 1073 (2004).
[33] V. Schmidt, H. Riel, S. Senz, S. Karg, W. Riess, and U. Gosele, Small **2**, 85 (2006).
[34] J. Goldberger, A. I. Hochbaum, R. Fan, and P. D. Yang, Nano Lett. **6**, 973 (2006).
[35] L. J. Lauhon, M. S. Gudiksen, D. Wang, and C. M. Lieber, Nature (London) **420**, 57 (2002).
[36] Y. Wu, R. Fong, and P. Yang, Nano Lett. **2**, 83 (2002).
[37] M. T. Bjork, B. J. Ohlsson, T. Sass, A. I. Persson, C. Thelander, M. H. Magnusson, K. Deppert, L. R. Wallenberg, and L. Samuelson, Nano Lett. **2**, 87 (2002).
[38] M. Gudiksen, L. Lauhon, J. Wang, D. C. Smith, and C. M. Lieber, Nature (London) **415**, 617 (2002).
[39] R. R. He, D. Gao, R. Fan, A. I. Hochbaum, C. Carraro, R. Maboudian, and P. D. Yang, Adv. Mater. (Weinheim, Ger.) **17**, 2098 (2005).
[40] I. Vasiliev, J. R. Chelikowsky, and R. M. Martin, Phys. Rev. B **65**, 121302(R) (2002).
[41] Z. Zhou, L. Brus, and R. Friesner, Nano Lett. **3**, 163 (2003).
[42] R. N. Musin and X.-Q. Wang, Phys. Rev. B **71**, 155318 (2005).
[43] Y. Wu, Y. Cui, L. Huynh, C. J. Barrelet, D. C. Bell, and C. M. Lieber, Nano Lett. **4**, 433 (2004).
[44] S. Hong and M. Y. Chou, Phys. Rev. B **57**, 6262 (1998).
[45] M. C. Payne, M. P. Teter, D. C. Allan, T. A. Arias, and J. D. Joannopoulos, Rev. Mod. Phys. **64**, 1045 (1992).

[46] G. Kresse and D. Joubert, Phys. Rev. B **59**, 1758 (1999).
[47] B. Lee and R. E. Rudd, Phys. Rev. B **75**, 041305(R) (2007)
[48] A. San Paulo, J. Bokor, R. T. Howe, R. He, P. Yang, D. Gao, C. Carraro, and R. Maboudian, Appl. Phys. Lett. **87**, 053111 (2005).
[49] J. P. Perdew, K. Burke, and M. Ernzerhof, Phys. Rev. Lett. **77**, 3865 (1996).
[50] H. J. McSkimin and P. Andreatch, J. Appl. Phys. **35**, 2161 (1964).
[51] S. Izumi, S. Hara, I. Kumagai, and S. Sakai, Thin Solid Films **467**, 253(2004).
[52] B. Lee and R. E. Rudd, Phys. Rev. B **75**, 195328 (2007).
[53] S. Horiguchi, Y. Nakajima, Y. Takahashi, and M. Tabe, Jpn. J. Appl. Phys., Part 1 **34**, 5489(1995).
[54] A. J. Williamson, J. C. Grossman, R. Q. Hood, A. Puzder, and G. Galli, Phys. Rev. Lett. **89**, 196803 (2002).
[55] I. Balslev, Phys. Rev. **143**, 636 (1966).
[56] K. Rim, J. Welser, J. L. Hoyt, and J. F. Gibbons, Tech. Dig. - Int. Electron Devices Meet. **1995**, 517.
[57] J. C. She, S. Z. Deng, N. S. Xu, R. H. Yao, and J. Chen, Appl. Phys. Lett. **88**, 13112 (2006).
[58] Y. Cui, Q. Wei, H. Park, and C. Lieber, Science **293**, 1289 (2001).
[59] B. Shan and K. J. Cho, Phys. Rev. Lett. **94**, 236602 (2005).